ADVANCES IN FOREST FIRE RESEARCH

2022

Edited by
DOMINGOS XAVIER VIEGAS
LUÍS MÁRIO RIBEIRO

Influence of Fuel Structure on Gorse Fire Behaviour

Andres Valencia*[1]; Katharine Melnik[1]; Nick Sanders[1]; Adam Sew Hoy[1]; Mozhi Yan[1]; Marwan Katurji[2]; Jiawei Zhang,[3,2]; Benjamin Schumacher[2]; Robin Hartley[3]; Samuel Aguilar-Arguello[3]; Grant Pearce[3,4]; Mark Finney[5]; Veronica Clifford[3]; Tara Strand[3]

[1]Department of Civil and Natural Resources Engineering, University of Canterbury, Christchurch 8140, New Zealand, {andres.valencia, katharine.melnik}@pg.canterbury.ac.nz
[2] University Center for Atmospheric Research, School of Earth and Environment, University of Canterbury, New Zealand {marwan.katurji, benjamin.schumacher}@pg.canterbury.ac.nz
[3] New Zealand Forest Research Institute, Scion, New Zealand {jiawei.zhang, robin.hartley, tara.strand, samuel.aguilar}@scionresearch.com
[4]Fire Emergency New Zealand {grant.pearce2@fireandemergency.nz}
[5]Forest Service, Missoula Fire Science Laboratory, United States of America {mark.finney@usda.gov)

** Corresponding author*

Keywords

Fire behaviour, wildfires, lidar, UAV, Image velocimetry

Abstract

Complex interactions between fuel structure and fire highly affects the fire spread efficiency and localized behaviour. Heterogeneous arrangement of the fuel coupled with variability in fuel characteristics can strengthen or hinder heat transfer efficiency, preheating of unburned fuel and consecutive ignition. In this study, we leverage recently developed non-intrusive unmanned aerial vehicle-based (UAV) methods to spatially resolved field-scale fire behaviour properties and compare them with the Canopy Height Model (CHM) derived from pre-burn lidar measurements. Rate of spread and flaming residence time are calculated and mapped from high-resolution overhead visible footages acquired during a four-hectare prescribed gorse fire. The proposed method allows for quantification of the influence of fuel structure spatial variation on fire behaviour properties by capturing localized fire front and burning time variations associated with negative ("gaps") and positive ("bumps") changes in canopy height. These findings are supported by results obtained from a novel fire flow visualization method based upon image velocimetry, described here for the first time. Complex fire flow is synthetised via 2D time-averaged motion streamlines and compared with CHM fuel structure. Results suggest that localized fire behaviour changes may be related to flow channelling effects induced by the presence of gaps, enhancing fire flow contact and overall heat transfer efficiency.

1. Introduction

Fire behaviour is driven by complex interactions between fire energy exchanges, fuel load and structure, and atmospheric processes (Clements et al., 2007; Dahale et al., 2013; Finney et al., 2015; Sullivan, 2017; Katurji et al., 2021). Understanding these interactions is essential for several critical aspects of wildfire sciences and for informed firefighting operations (Beer, 1991; Page and Butler, 2017), building design in the Wildland Urban Interface (WUI) (Penney, Habibi and Cattani, 2020; Penney et al., 2022) and development of wildfire simulation models (Mell et al., 2007, 2011; Morvan, 2011; Hoffman et al., 2016). Field-scale fire behaviour has primarily been characterised through experimental and analytical properties describing the overall behaviour of the fire (e.g. average rate of spread, residence time and fire intensity) generally accounting for first-order mechanisms. Although this practical approach is deemed reasonable for numerous applications, it falls short of the required level of detail necessary to progress the current knowledge on fire spread mechanisms (Martins Fernandes, 2001; Santoni et al., 2006; Cruz et al., 2013) and to assess the ability of the physics-based models (e.g. WFDS and FireTEC) to predict fire behaviour, among others.

Several efforts have been made to develop deployable techniques able to accurately characterize spatial and transient fire behaviour and their interactions with fuel and overlying atmosphere at field scale. Rossi et al. (2010) developed a 3D imaging technique capable of measuring morphological characteristics of the fire and estimate ROS of complex fire fronts. This technique has been expanded to include UAV technology (Ciullo,

Rossi and Pieri, 2020) aiming to enhance spatial coverage and fire geometry definition, as well as exploring fuel/fire interactions. Recently, Katurji et al. (2021) developed a novel velocimetry technique based upon high-resolution infrared images suitable for understanding fire/atmospheric interactions between the flaming zone and the overlying atmospheric turbulent boundary layer. The technique was tested during stubble wheat prescribed fires and validated with in-field instrumentation.

These aforementioned capabilities are examples of a new generation of experimental techniques capable of capturing complex wildfire interactions at field scale, and they will contribute to further characterising the dynamics of the flaming zone which is essential for the development of future fire spread models. In this context, we present an experimental study of spatially-resolved fire behaviour properties at field scale linked to high fidelity fuel structure derived from pre-burn UAV lidar (ULS) measurements. We leverage on recently developed non-intrusive UAV-based methods to study the influence of fuel structure (canopy height and spatial arrangement) from pre-burn ULS on fire behaviour (rate of spread and flaming residence time) derived high-resolution overhead RGB videos during a four-hectare prescribed gorse fire. Because of word-limit constraints, we only summarize the non-intrusive experimental methods used in this research (Section 2) and we present and comment the derived maps Rate of Spread (ROS) and Flaming Residence Time (FRT) (section 3) in this short paper.

2. Experiments and Methods

2.1. Site description and burning conditions

The research site is located at -43.409, 171.568, 15 km south of the Rakaia Gorge in Mid-South Canterbury, New Zealand. A 200 m × 200 m burn plot was established on flat ground (a dry riverbed with slight undulations), ensuring that it aligns with the prevailing wind directions. The overstory was made up of gorse (*Ulex europaeus* L.) with a small component of matagouri (*Discaria toumatou* Raoul), and the understory consisted of mostly grasses with a component of rose (*Rosa* sp.), California thistle (*Cirsium arvense* (L.) Scop) and Russell lupin (*Lupinus polyphyllus* Lindl). Gorse height ranged from 0.2 m to 2.0 m, and its density and distribution was heterogeneous across the site, with some areas containing tall dense vegetation, and other areas being relatively open with short clumps of gorse interspersed with grassy patches.

The burn was ignited on 2nd March 2020 at 12:11pm and lasted 5 minutes. The mean temperature was 22.9 °C, mean relative humidity was 33.2%, mean wind direction was 311.2° and mean wind speed was 9.8 m/s (35.28 km/hr) as recorded by the on-site 10-meter weather station.

2.2. UAV and lidar Acquisition

UAVs capabilities were used for two different purposes: to record nadir RGB videos of the flaming zone and to obtain a pre-burn high-density point cloud from a ULS. In advance of any flight operations, an extensive set of ground control points (GCPs) was established throughout the study site. Eight ground control points evenly distributed across the study area ensured a suitable level of accuracy of the ULS data. Furthermore, 36 ground control points were established around the individual research burn blocks to be used during the georectification of the acquired frames from the visual imagery and the alignment of the two data streams.

Aerial video data of the flame zone was captured using a DJI Zenmuse XT2 dual thermal RGB sensor with integrated 1/17 inch 12MP RGB camera (DJI Ltd., Shenzhen, China), mounted on a DJI Matrice 210 UAV (DJI Ltd., Shenzhen, China). Video was captured in MP4 format at a framerate of 30 fps. Pre-burn ULS data was captured with a LidarUSA Snoopy V-series system (Fagerman Technologies, INC., Somerville, AL, USA), that incorporates a Riegl MiniVUX-1 UAV scanner (Riegl, Horn, Austria). This sensor was attached to a DJI Matrice 600 Pro UAV (DJI Ltd., Shenzhen, China).

Figure 1. Pilot taking off Matrice 210 with DJI XT2 camera prior to burn commencing; b. Setting up Matrice 210 UAV; c. DJI Matrice 600 craft taking off, carrying MiniVUX lidar sensor as payload.

Processing of the raw point cloud from Lidar was then carried out using two pieces of software. First, the point cloud was tiled and had basic noise filtering applied using the LasTools software version 210,418 (Isenburg, 2014). The tiles output from LasTools were then imported into the R statistical software version 4.0.4 (R Core Team, 2020) and processed using a data processing pipeline developed using the LidR library (Roussel et al., 2018). First ground points were classified and then a digital terrain model (DTM) with a resolution of 1 m was derived from these points. The point cloud was then height-normalised using the DTM, more noise filtering was applied to remove spurious points, and finally a pit-free canopy height model (CHM) with a resolution of 0.25 m was calculated.

3. Description of Techniques

3.1. Flame Residence Time and Fire Perimeter Tracking

In order to calculate the residence time and the pixel-wise rate of spread (ROS) of the fire, the Fire Perimeter Tracking algorithm (Melnik 2021, Schumacher et al. 2021) was used. First, each frame of the stabilized RGB videos was analysed to identify which pixels contain active flames. This was done by manually identifying colour thresholds in the hue, saturation and value (HSV) colour space that indicate the presence of flames in a given pixel. Using the location of active flaming in each video frame, two two-dimensional arrays were created: (1) the ignition array, each pixel of which contained the first timestamp of active flaming in the given pixel of the burn plot, and (2) the extinction array, each pixel of which contained the last timestamp of active flaming. The ignition array was subtracted from the extinction array in order to create the flame residence time array, which contained the burning duration of each pixel across the burn plot.

In order to calculate the pixel-wise rate of fire spread, a 41×41 pixel moving window was established across the ignition array, with every pixel of the ignition array taking its turn to serve as the centre pixel of the moving window. Within the moving window, only timestamps immediately preceding or following the timestamp of the central pixel were retained. Vectors going from the preceding-timestamp pixels to the central pixel, and advancing from the central pixel to the following-timestamp pixels were calculated, and these vectors were averaged to obtain the rate and direction of spread of the central pixel. The window then moved over and the process was repeated for the next pixel in the ignition array to serve as the centre pixel. The resulting array contained the computed rate and direction of fire perimeter spread for each pixel in the burn plot.

3.2. Fire Flow Streamlines visualization and Image Velocimetry

Image Velocimetry was used to derive and map the displacement of fire features from consecutive RGB frames. The method (Schumacher et al. 2021), which has originally been developed for flow velocimetry estimations from infrared image analysis, has been successfully applied in this work to visualise gorse fire flow from RGB images, and to compare it with fuel structure. The technique uses greyscale image processing to estimate direction and magnitude of the displacement of the observed fire features between two consecutive frames (1/30

s). The resulting vectorial field was then derived to calculate the corresponding flow streamlines and visualize the fire flow.

4. Results

4.1. Description of Fuel Structure and Fire Behaviour

Figure 2a shows an image of the fire extracted from the RGB UAV footage ~1 min after ignition. The figure highlights the observable flaming zone and fire front once the acceleration phase is ended. The length of the observable fire in the streamwise direction $y+$, or flaming zone depth, was found to variate across the width of the plot, ranging from ~10 m in regions of low canopy height to ~50 m in regions of high canopy height. Fire spread was characterized by quick progressions of the fire front involving intermittent coverage and subsequent ignition of immediate preheated unburned fuel, resulting in localized progression in short periods of time.

Figure 2b shows the pre-burn CHM obtained from ULS data. The plot was heterogeneous involving interspersed zones of high and low canopy height, with and averaged CHM of 0.75 m and a high standard deviation of ± 0.56, representing 75% of the average value. The right side of the plot was mostly composed of low height fuel with sporadic sectors of high fuel (e.g. dotted line), whereas the opposite occurred in most of the left side of the plot (e.g. dashed line).

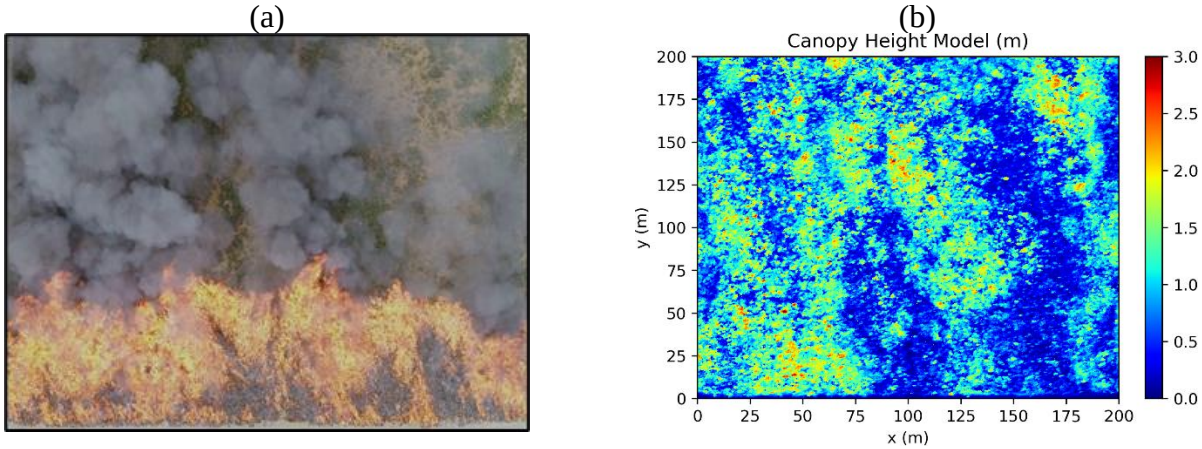

Figure 2. Collected datasets of the burn plot where the ignition took place along the bottom of the x-axis, with the x-axis showing plot width in meters, the y-axis showing the plot length in meters, and the value corresponding to (a) the colour sensed with the UAV-mounted RGB videos, plan view, (b) the height of the vegetation canopy obtained from ULS data. The resolution of the CHM is $7.8 \cdot 10^{-2}$ m/pixel

Figure 3a and Figure 3b show the fire behaviour properties estimated in this study. FRT, shown in Figure 3a, ranged between approximately 10 s to 1.5 min with very high values at the plot edges where liquid fuel was used for ignition purposes. Through qualitative comparison with CHM, FRT seems to present longer flaming combustion in regions of high canopy height. For instance, this pattern can be observed in the bottom-left (x = 50 m y = 25 m) and bottom-right (x = 175 m y = 25 m) sections of the maps. We hypothesize this behaviour results from high canopy height locations linked with high biofuel content participating in the combustion, relationship confirmed through analysis of pre-burn destructive samples. ROS, presented in Figure 3b, was found to be low during the first approximate 20 m where the fire was transitioning from an accelerating fire front with a small flaming zone to the established quasi-steady fire shown in Figure 2a. The ROS map captured the previously described quick progressions of the fire front as localized high ROS values. We hypothesize this could be explained by the presence of greater flame heights and longer fire activity in regions with higher canopy height, most likely associated with higher fuel load.

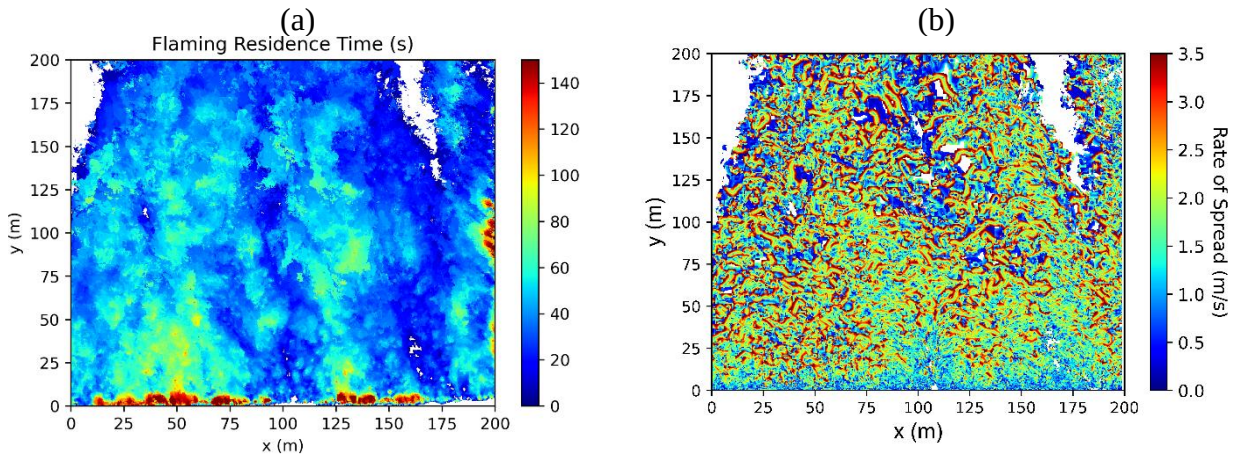

Figure 3. Derived datasets of the burn plot where the ignition took place along the bottom of the x-axis, with the x-axis showing plot width in meters, the y-axis showing the plot length in meters, and the value corresponding to (c) the rate of fire spread derived from the video footage, and (d) flame residence time also derived from the footage. The resolution of both maps is $7.8 \cdot 10^{-2}$ m/pixel

5. Acknowledgments, Samples, and Data

We would like to give a special thanks to all field support teams including technical and general staff. We also thank landowner for their various contributions leading to the success of the field campaigns. University of Canterbury research team would like to acknowledge the very thoughtful, well organized, and proactive support we have received from all the volunteering firefighting crew. The success of our experiments and the safety of our science crew can only be partially attributed to our design but greatly attributed to the safe and well-executed plan from the volunteer crew. A special thanks to the Scion field crew: David Glogoski, Max Novoselov, Richard Parker, Brooke O'Connor, Emma Percy, and Ilze Pretorius. We would also like to acknowledge Peter Massam from Scion's UAV team for assistance with UAV data capture and processing. This research was co-funded by Ministry of Business, Innovation and Employment (MBIE), New Zealand, grant number C04X1603 entitled "Preparing New Zealand for Extreme Fire" and grant number C04X2103 "Extreme wildfire: Our new reality - are we ready?"

6. References

Beer, T. (1991) 'Bushfire rate-of-spread forecasting: Deterministic and statistical approaches to fire modelling', Journal of Forecasting, 10(3), pp. 301–317. doi:10.1002/for.3980100306.

Clements, C.B. et al. (2007) 'OBSERVING THE DYNAMICS OF WILDLAND GRASS FIRES', Bulletin of the American Meteorological Society, 99(7), pp. 1369–1382.

Cruz, M.G. et al. (2013) 'Fire behaviour modelling in semi-arid mallee-heath shrublands of southern Australia', Environmental Modelling and Software, 40, pp. 21–34. doi:10.1016/j.envsoft.2012.07.003.

Dahale, A. et al. (2013) 'Effects of distribution of bulk density and moisture content on shrub fires', International Journal of Wildland Fire, 22(5), pp. 625–641. doi:10.1071/WF12040.

Finney, M.A. et al. (2015) 'Role of buoyant flame dynamics in wildfire spread', Proceedings of the National Academy of Sciences of the United States of America, 112(32), pp. 9833–9838. doi:10.1073/pnas.1504498112.

Hoffman, C.M. et al. (2016) 'Evaluating Crown Fire Rate of Spread Predictions from Physics-Based Models', Fire Technology, 52(1), pp. 221–237. doi:10.1007/s10694-015-0500-3.

Isenburg, M. (2014) 'LAStools-efficient LiDAR processing software', Available online: lastools. org (accessed on 10 October 2017) [Preprint].

Katurji, M. et al. (2021) 'Turbulent Thermal Image Velocimetry at the Immediate Fire and Atmospheric Interface', Journal of Geophysical Research: Atmospheres, 126(24), pp. 1–14. doi:10.1029/2021JD035393.

Martins Fernandes, P.A. (2001) 'Fire spread prediction in shrub fuels in Portugal', Forest Ecology and Management, 144(1–3), pp. 67–74. doi:10.1016/S0378-1127(00)00363-7.

Mell, W. et al. (2007) 'A physics-based approach to modelling grassland fires', International Journal of Wildland Fire, 16(1), pp. 1–22. doi:10.1071/WF06002.

Morvan, D. (2011) 'Physical Phenomena and Length Scales Governing the Behaviour of Wildfires: A Case for Physical Modelling', Fire Technology, 47(2), pp. 437–460. doi:10.1007/s10694-010-0160-2.

Page, W.G. and Butler, B.W. (2017) 'An empirically based approach to defining wildland firefighter safety and survival zone separation distances', International Journal of Wildland Fire, 26(8), pp. 655–667. doi:10.1071/WF16213.

Penney, G. et al. (2022) 'The CAED Framework for the Development of Performance-Based Design at the Wildland–Urban Interface', Fire, 5(2), pp. 1–19. doi:10.3390/fire5020054.

Penney, G., Habibi, D. and Cattani, M. (2020) A handbook of wildfire engineering: guidance for wildfire suppression and resilient urban designHabibi, Daryoush Cattani, Marcus, Bushfire and Natural Hazards CRC. Edited by B. CRC and N. Hazards. Melbourne. Available at: https://www.bnhcrc.com.au/publications/handbook-of-wildfire-engineering.

Rossi, L. et al. (2010) 'A 3D vision system for the measurement of the rate of spread and the height of fire fronts', Measurement Science and Technology, 21(10). doi:10.1088/0957-0233/21/10/105501.

Roussel, J.-R. et al. (2018) 'lidR: Airborne LiDAR data manipulation and visualization for forestry applications', R package version, 1(1).

Santoni, P.A. et al. (2006) 'Instrumentation of wildland fire: Characterisation of a fire spreading through a Mediterranean shrub', Fire Safety Journal, 41(3), pp. 171–184. doi:10.1016/j.firesaf.2005.11.010.

Schumacher, B. et al. (2022) 'Rate of spread and flaming zone velocities of surface fires from visible and thermal image processing', International Journal of Wildland Fire (in press) [Preprint].

Sullivan, A.L. (2017) 'Inside the Inferno: Fundamental Processes of Wildland Fire Behaviour: Part 2: Heat Transfer and Interactions', Current Forestry Reports, 3(2), pp. 150–171. doi:10.1007/s40725-017-0058-z.

Vacca, P. et al. (2020) 'WUI fire risk mitigation in Europe: A performance-based design approach at home-owner level', Journal of Safety Science and Resilience, 1(2), pp. 97–105. doi:10.1016/j.jnlssr.2020.08.001.